

# Journal Pre-proof

Fabrication and thermal conductivity of  $\text{CeO}_2\text{-Ce}_3\text{Si}_2$  composite

Jungsu Ahn, Gyeonghun Kim, Yunsong Jung, Sangjoon Ahn

PII: S1738-5733(20)30094-2

DOI: <https://doi.org/10.1016/j.net.2020.07.016>

Reference: NET 1228

To appear in: *Nuclear Engineering and Technology*

Received Date: 31 January 2020

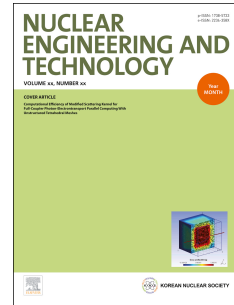
Revised Date: 27 June 2020

Accepted Date: 12 July 2020

Please cite this article as: J. Ahn, G. Kim, Y. Jung, S. Ahn, Fabrication and thermal conductivity of  $\text{CeO}_2\text{-Ce}_3\text{Si}_2$  composite, *Nuclear Engineering and Technology* (2020), doi: <https://doi.org/10.1016/j.net.2020.07.016>.

This is a PDF file of an article that has undergone enhancements after acceptance, such as the addition of a cover page and metadata, and formatting for readability, but it is not yet the definitive version of record. This version will undergo additional copyediting, typesetting and review before it is published in its final form, but we are providing this version to give early visibility of the article. Please note that, during the production process, errors may be discovered which could affect the content, and all legal disclaimers that apply to the journal pertain.

© 2020 Korean Nuclear Society, Published by Elsevier Korea LLC. All rights reserved.



## Fabrication and Thermal Conductivity of CeO<sub>2</sub>-Ce<sub>3</sub>Si<sub>2</sub> Composite

Jungsu Ahn<sup>a</sup>, Gyeonghun Kim<sup>a</sup>, Yunsong Jung<sup>a</sup>, Sangjoon Ahn<sup>a</sup>

<sup>a</sup>Department of Nuclear Engineering, Ulsan National Institute of Science and Technology, Ulsan, Ulsan 44919, Republic of Korea

---

### Abstract

Various compositions of CeO<sub>2</sub>-Ce<sub>3</sub>Si<sub>2</sub> (0, 10, 30, 50, and 100 wt%Ce<sub>3</sub>Si<sub>2</sub>) composites were fabricated using conventional sintering and spark plasma sintering. Lower relative density, enhanced interdiffusion of oxygen and silicon, and silicide agglomerations from the congruent melting of Ce<sub>3</sub>Si<sub>2</sub> at 1390 °C were only observed from conventionally-sintered pellets. Thermal conductivity of spark plasma sintered CeO<sub>2</sub>-Ce<sub>3</sub>Si<sub>2</sub> composites was calculated from the measured thermal diffusivity, specific heat, and density, which exhibited dense (> 90 %TD) and homogeneous microstructure. The composite with 50 wt%Ce<sub>3</sub>Si<sub>2</sub> exhibited 55% higher thermal conductivity than CeO<sub>2</sub> at 500 °C, and 81% higher at 1000 °C.

**Keywords:** Cerium oxide, Cerium silicide, Composite, Spark plasma sintering, Thermal conductivity

---

### 1. Introduction

Autonomous, Transportable, On-demand reactor-Module or '*ATOM*', is a conceptual soluble-boron-free small modular water-cooled reactor that enables passive daily load following operation (PDLFO) by autonomous frequency control, which requires lower fuel temperature than conventional LWRs to obtain less negative fuel temperature coefficient (FTC) [1]. UO<sub>2</sub>-based composite fuel mixed with high thermal conductivity additives is considered for the reactor design to concurrently achieve enhanced fuel thermal conductivity, increased uranium loading, and reasonable corrosion resistance.

Increased uranium loading narrows the material selection down to uranium compounds such as UN, UC, and U<sub>3</sub>Si<sub>2</sub>, which all have higher thermal conductivity and fissile density than those of UO<sub>2</sub> [2-4]. Uranium sesquisilicide (U<sub>3</sub>Si<sub>2</sub>) was the first selected additive for this study owing to relatively better oxidation resistance among the uranium compounds, and it

also has 4-8 times higher thermal conductivity and 16% higher fissile density compared to  $\text{UO}_2$  [3].

Density-specific thermal conductivity database of the composite, which is the eventual goal of this study, is first required for candidate fuel compositions to examine the viability of the autonomous reactor design with  $\text{UO}_2\text{-U}_3\text{Si}_2$  fuel. Surrogate material was, however, first tested to develop the fabrication process for the composite fuel while minimizing uranium-bearing waste generation. Among several surrogate elements, cerium (Ce) was selected since  $\text{CeO}_2$  and  $\text{Ce}_3\text{Si}_2$  have the same crystal structures with  $\text{UO}_2$  and  $\text{U}_3\text{Si}_2$ , respectively [5-8]. The cerium compounds also have similar thermal conductivities and melting temperatures with their uranium counterparts [9-13]. In particular, the ratios between melting temperatures of  $\text{CeO}_2/\text{Ce}_3\text{Si}_2$  (2490 °C/1390 °C) and  $\text{UO}_2/\text{U}_3\text{Si}_2$  (2865 °C/1660 °C) were expected to be close enough to glimpse the sintering behavior of  $\text{UO}_2\text{-U}_3\text{Si}_2$  composite.

In this study, various compositions of  $\text{CeO}_2\text{-}x\text{Ce}_3\text{Si}_2$  ( $x = 0, 10, 30, 50, \text{ and } 100 \text{ wt\%}$ ) composite pellets were fabricated using conventional sintering (CS) and spark plasma sintering (SPS) with varying sintering temperatures (1000, 1200, 1400, and 1600 °C). The resulted density and microstructure of  $\text{CeO}_2\text{-Ce}_3\text{Si}_2$  composites were compared to optimize the parameters for each sintering method. The thermal conductivity of spark plasma sintered high density (> 90 %TD) composite pellets were measured using laser flash analyzer (LFA) up to 1000 °C.

## 2. Material and methods

### 2.1. Sample preparation

Cerium sesquisilicide was synthesized utilizing high energy ball milling (HEBM) method, referring to G.A. Alanko *et al* [12]. The starting materials were high purity elemental Ce powder (~45  $\mu\text{m}$ , 99.9%, Avention) and Si powder (~1  $\mu\text{m}$ , 99.9995%, Avention). Material handling and sintering was conducted in a glove box under an argon atmosphere with less than 10 ppm  $\text{O}_2$  and  $\text{H}_2\text{O}$  to suppress rapid oxidation and ignition of flammable Ce and  $\text{Ce}_3\text{Si}_2$  powders. The synthesis was performed using a planetary ball mill (Fritsch PUVERISETTE 6, Germany) with 5- and 10-mm diameter milling media in 80 ml  $\text{ZrO}_2$  inert

atmosphere milling vessel. The elemental Ce and Si powder were loaded into milling vessel with 3:2 molar ratio, with milling media of 10:1 ball-to-powder ratio. The milling process was carried out at 550 rpm for 12 h, followed by 1 h milling and 5 min break. The milled powder attached to the vessel wall was collected by additional milling with acetone at 400 rpm for 30 min and the resulted mixture was vaporized to obtain  $\text{Ce}_3\text{Si}_2$  powder. The microstructure and phase of the as-milled powder were characterized using scanning electron microscope (Quanta200 FEG SEM, FEI, USA) and X-ray diffraction (XRD, D/MAX-2500, Rigaku, Japan). It needs to be noted that the XRD samples were prepared in a bulk form of 1 mm high pellet, which was spark plasma sintered at 600 °C for 5 min, to address the flammability issue of  $\text{Ce}_3\text{Si}_2$  powder in air.

## 2.2. Sintering

As-received  $\text{CeO}_2$  powder ( $\sim 1 \mu\text{m}$ , 99.9%, Avention) shown in Fig. 1 was homogeneously blended with 0/10/30/50/100 wt% of as-milled  $\text{Ce}_3\text{Si}_2$  powder using 3d tubular mixer at 150 rpm for 30 min. For the CS of the composite,  $\sim 57\%$  TD green pellets were prepared from cold compacting the mixed powder with 300 MPa in 12.7 mm diameter stainless steel die for 1 min. The green pellets were then sintered using a tube furnace (Nabertherm GmbH, Germany) at various temperatures (1000, 1200, 1400, and 1600 °C) for 6 h under an Ar atmosphere; 5 °C/min ramping rates and alumina ( $\text{Al}_2\text{O}_3$ ) crucible were adopted for all sintering temperatures. The SPS of the composite was carried out using DrSinter SPS-211LX. The mixed powder was loaded into 9.5 mm diameter graphite mold of which inside was wrapped with graphite foil to avoid sample-mold reaction, and then heated up to the same sintering temperatures with CS; however, with different ramping rate (80 °C/min), holding time (10 min), and atmosphere (vacuum), under 45 MPa of biaxial pressure. The SPS system temperature was monitored through a 0.5 mm diameter hole at the center of graphite mold using focused infrared pyrometer.

As-fabricated composite pellet density was measured using Archimedes immersion method with ethyl alcohol ( $\text{C}_2\text{H}_5\text{OH}$ ), and validated with measured density with mass divided by measured volume. The pellet morphology was observed using an optical microscope (OM, DM2700M, Leica, Japan) and SEM (SU8220, Hitachi, Japan). The phase characterization

was carried out by energy dispersive spectrometry (EDS) and XRD (D8 advanced, Bruker AXS, USA) with 20-80° 2 $\theta$  angle.

### 2.3. Thermal conductivity measurements

Thermal diffusivity and specific heat of the SPS pellets of CeO<sub>2</sub>-*x*Ce<sub>3</sub>Si<sub>2</sub> (*x* = 0, 10, 30, 50, and 100 wt%), sintered at 1000, 1200, and 1400 °C, were measured up to 1000 °C under an Ar atmosphere using LFA (LFA467HT, Netzsch, Germany); each measurement was repeated three times. The LFA samples were 9.8 mm in diameter and ~1.5 mm high, and graphite sprayed to increase Xenon laser absorptivity and emissivity. Thermal conductivity of the composite pellets was calculated from measured pellet density, average thermal diffusivity, and specific heat, using the equation (1),

$$\lambda(T) = \alpha(T) \cdot C_p(T) \cdot \rho(T) \quad (1)$$

where  $\lambda$  is thermal conductivity,  $\alpha$  is average thermal diffusivity,  $C_p$  is heat capacity, and  $\rho$  is measured density. Pellet density change during the measurement was tracked using a dilatometer (DIL-402C, Netzsch, Germany) and used to correct the measured density.

## 3. Results

### 3.1. Powder characterization

As-received CeO<sub>2</sub> powder with an average size of ~2  $\mu$ m and conventionally sintered CeO<sub>2</sub> pellet at 1600 °C for 6 h are indicated at Fig. 1. The morphology of metallic Ce powder (spherical) and as-milled Ce<sub>3</sub>Si<sub>2</sub> powder (arbitrary, 0.1-3  $\mu$ m), and Ce<sub>3</sub>Si<sub>2</sub> pellet are shown in Fig. 2. The XRD peaks of the starting materials, Ce and Si, and as-milled Ce<sub>3</sub>Si<sub>2</sub> powder shown in Fig. 3 were identified referring to Inorganic Crystal Structure Database (ICSD) [15]; likely tetragonal Ce<sub>3</sub>Si<sub>2</sub> with secondary off-stoichiometric Ce<sub>5</sub>Si<sub>4</sub> and Ce<sub>2</sub>O<sub>3</sub> phases. A few missing primary diffraction peaks of Ce<sub>3</sub>Si<sub>2</sub> could be attributed to crystallographic texture of bulk XRD sample resulted from spark plasma sintering under high pressure.

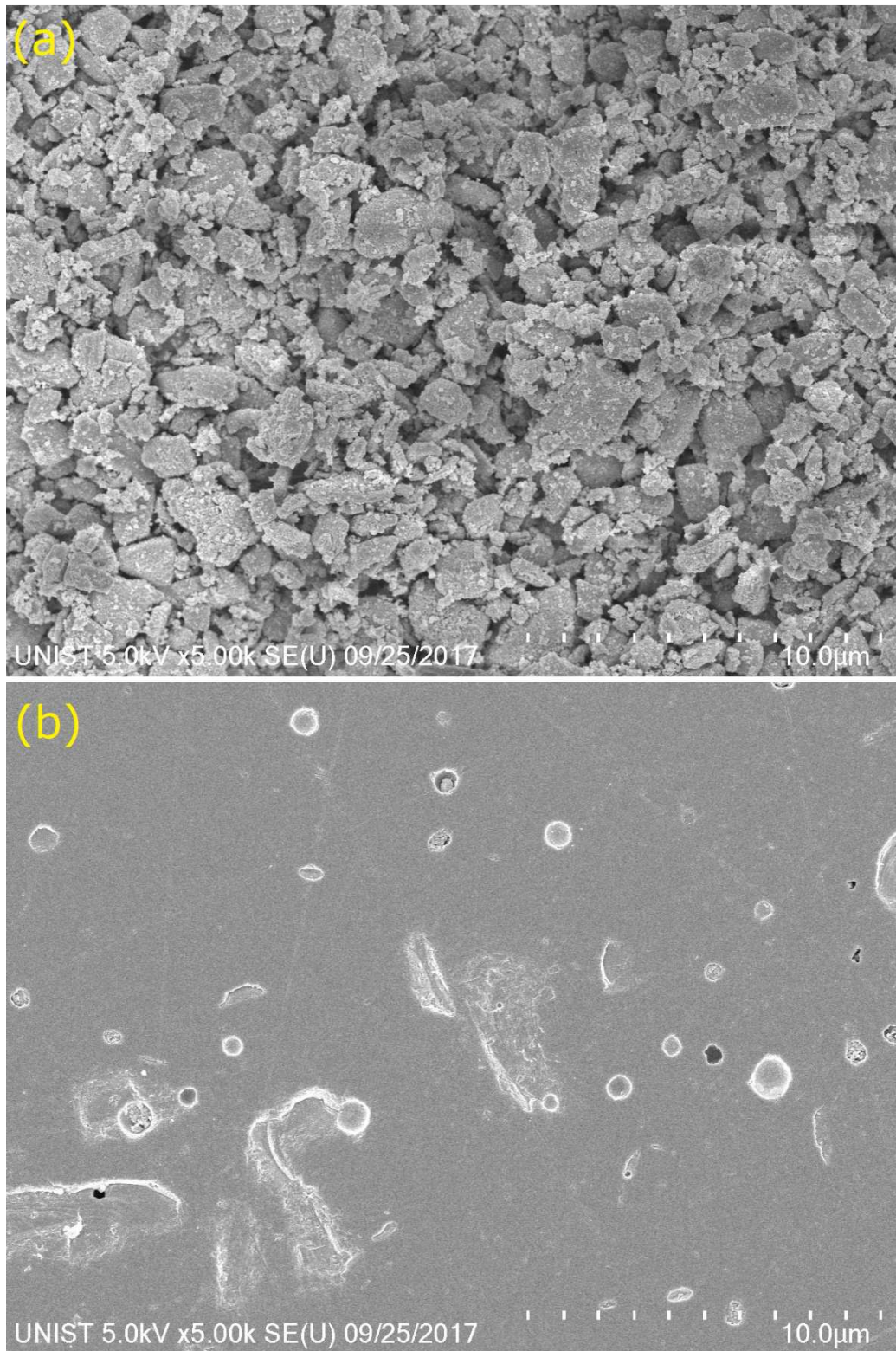


Figure 1: SEM image of (a) as-received  $\text{CeO}_2$  powder, (b) conventionally sintered  $\text{CeO}_2$  pellet (1600  $^\circ\text{C}$ , 6 h)

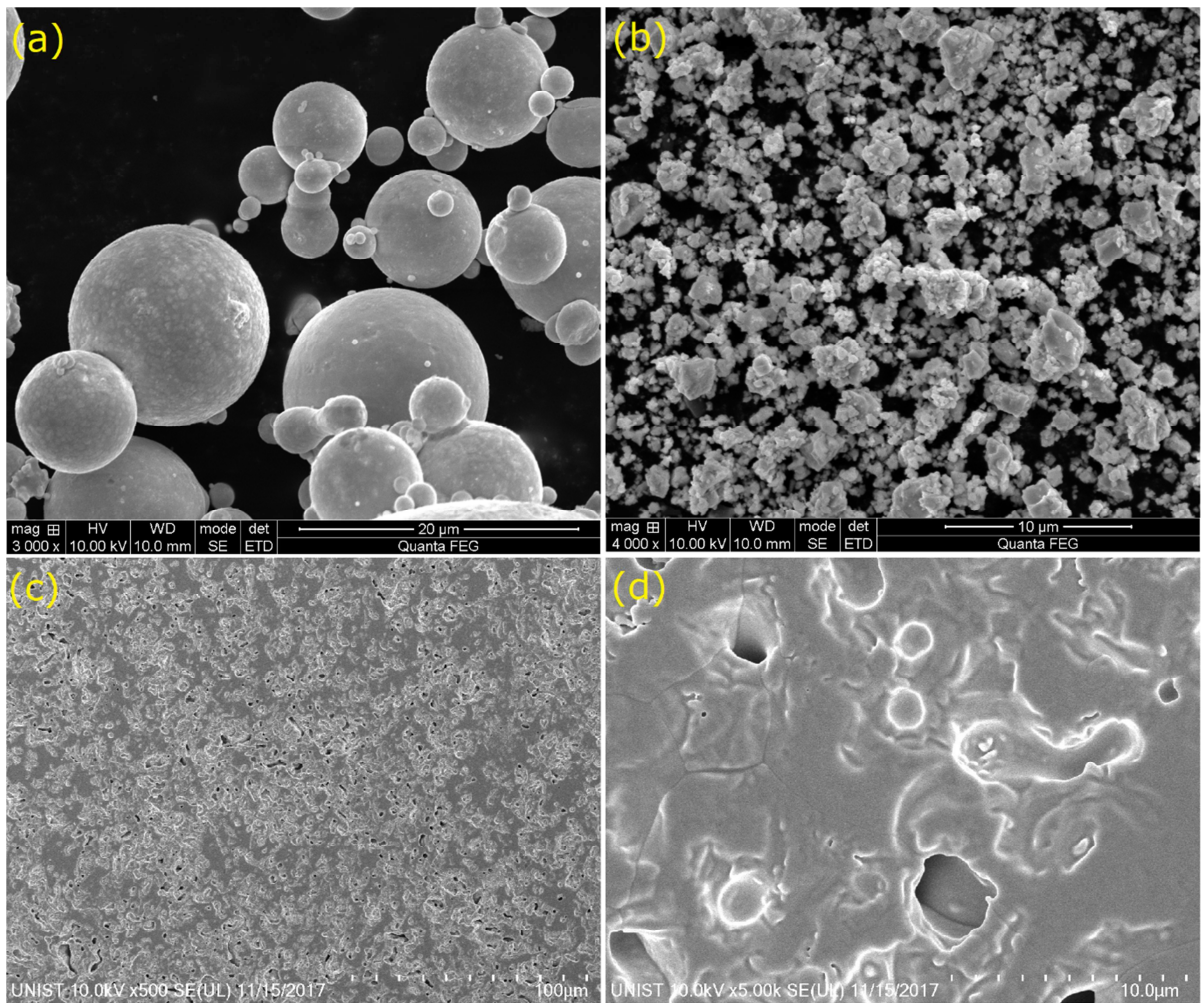


Figure 2: SEM image of (a) as-received Ce metal powder, and (b) Ce<sub>3</sub>Si<sub>2</sub> powder, (c) and (d) conventionally sintered Ce<sub>3</sub>Si<sub>2</sub> pellet (1200 °C, 6h)

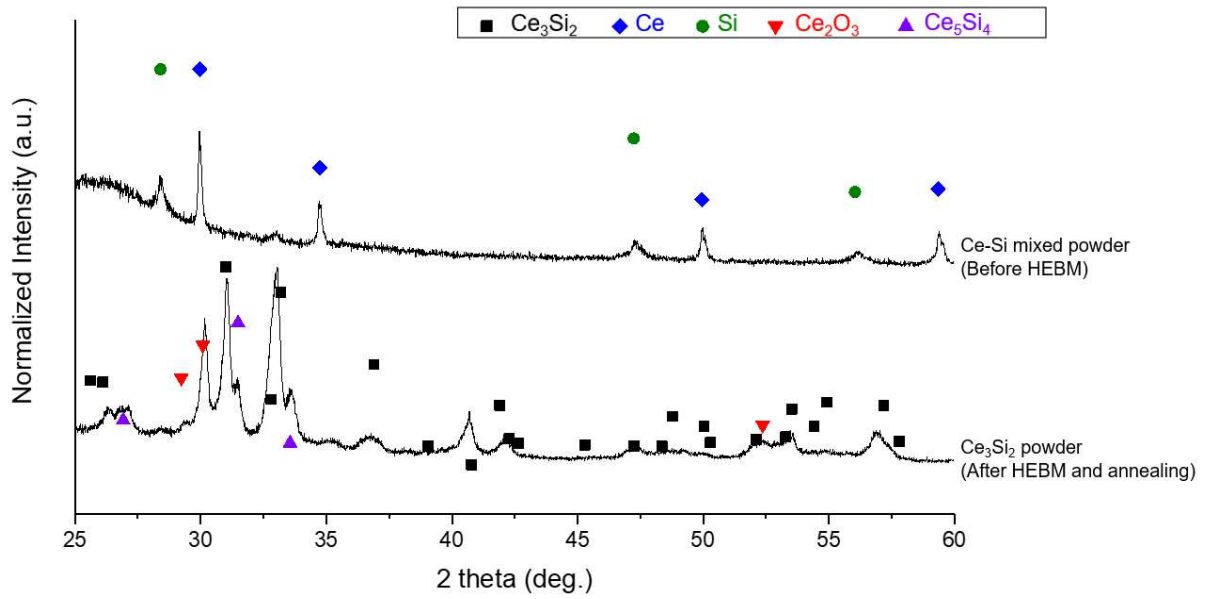


Figure 3: XRD diffraction pattern for homogeneously mixed Ce-Si powder and HEBM synthesized Ce<sub>3</sub>Si<sub>2</sub> powder with 24 h annealing at 800 °C.

### 3.2. Pellet characterization

Figure 4 shows the XRD analysis of CeO<sub>2</sub> powder and CeO<sub>2</sub>-30 wt%Ce<sub>3</sub>Si<sub>2</sub> composites fabricated by CS and SPS. Both sintering methods yielded similar results which indicate the formation of Ce<sub>2</sub>O<sub>3</sub>, but much higher peak for CS .



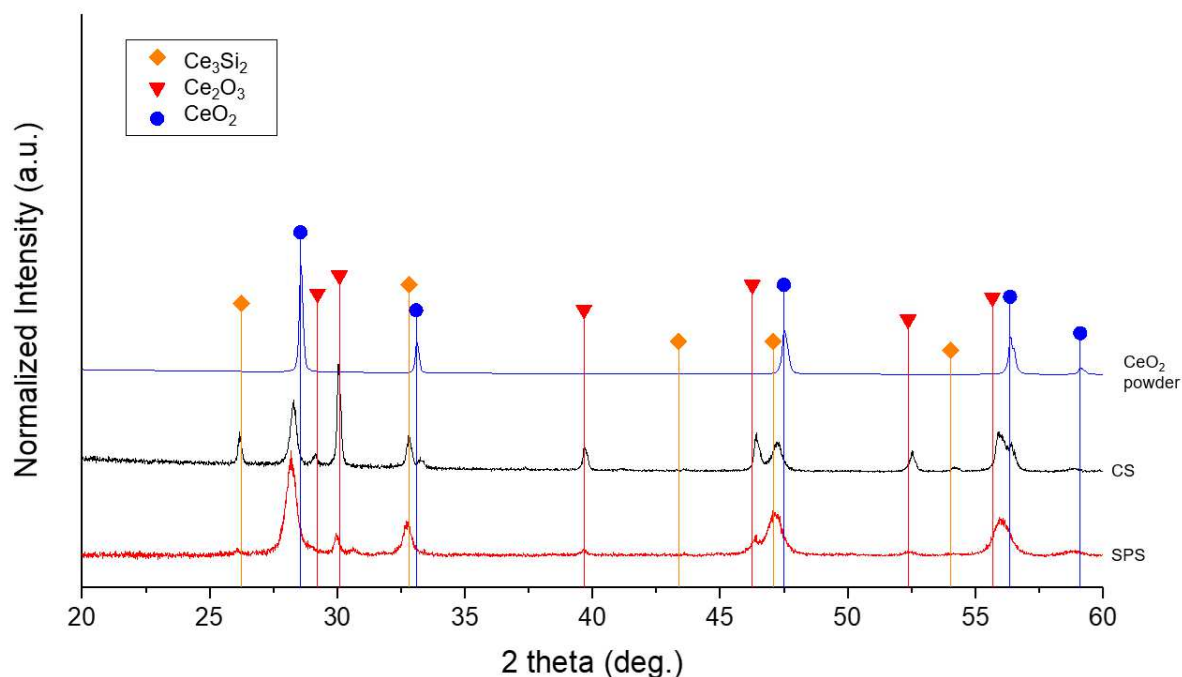


Figure 4: XRD diffraction pattern for  $\text{CeO}_2$ -30 wt% $\text{Ce}_3\text{Si}_2$  pellets sintered by CS at 1600 °C for 6 h and SPS at 1400 °C for 10 min.

The sintered pellet density was measured using Archimedes' principle, and the relative density for four different sintering temperatures (1000, 1200, 1400, and 1600 °C) are displayed in Fig 5; data for conventionally sintered 100wt%  $\text{Ce}_3\text{Si}_2$  pellet are not included due to partial melt, sequential loss of mixed powder from the mold. Spark plasma sintering always yielded higher density (83 ~ 96 %TD) pellets compared to CS at the same sintering temperature, and pellet densities were increasing monotonically with increasing sintering temperature for both methods. For CS pellets, however, density increase with elevated sintering temperature was remarkable, from ~62 %TD for 1000 °C to ~92%TD for 1600 °C, especially at high sintering temperature which seems to be the effect of liquid phase sintering. In contrast, sintering temperature effect for SPS tends to saturate at 1200 °C, especially for silicide-rich (> 30 wt% $\text{Ce}_3\text{Si}_2$ ) pellets. For CS, single phase  $\text{CeO}_2$  showed the highest relative density, while 10 wt% $\text{Ce}_3\text{Si}_2$  showed the lowest.

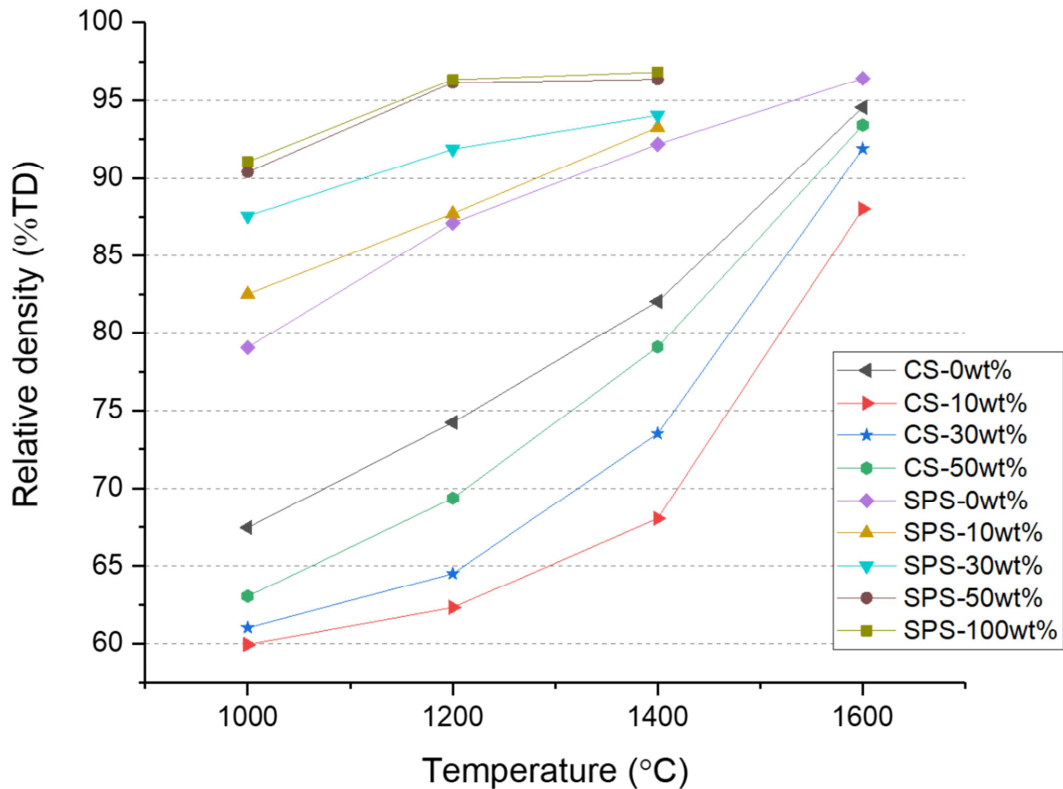


Figure 5: Relative density of conventionally and spark plasma sintered composite pellets with varying sintering temperature and  $\text{Ce}_3\text{Si}_2$  composition.

The OM and SEM images of the 30 wt% $\text{Ce}_3\text{Si}_2$  composite pellet sintered at 1600 °C are given in Fig. 6, which representatively shows the characteristic microstructure of CS pellets, bulk composite matrix with submillimeter metallic inclusions surrounded with interaction area, which are comprised of numerous submicron hexagonal particles. The EDS mapping on the inclusion (Fig. 7) shows silicon enrichment for the inclusion and depletion from the bulk. This metallic inclusions was rarely observed from the SPS pellets; a rather homogeneous distribution of silicide within oxide matrix, almost without pores, is well shown in Fig. 8. The EDS mapping of  $\text{CeO}_2$ -30 wt% $\text{Ce}_3\text{Si}_2$  (Fig. 9) also shows clear phase boundary and limited oxygen presence in the SPS pellet in contrast to diffused phase boundary and near

homogeneous oxygen distribution in the CS pellet. Both composite pellets sintered by CS and SPS method did not show distinct interaction layer between the interface of  $\text{CeO}_2$  and  $\text{Ce}_3\text{Si}_2$ .

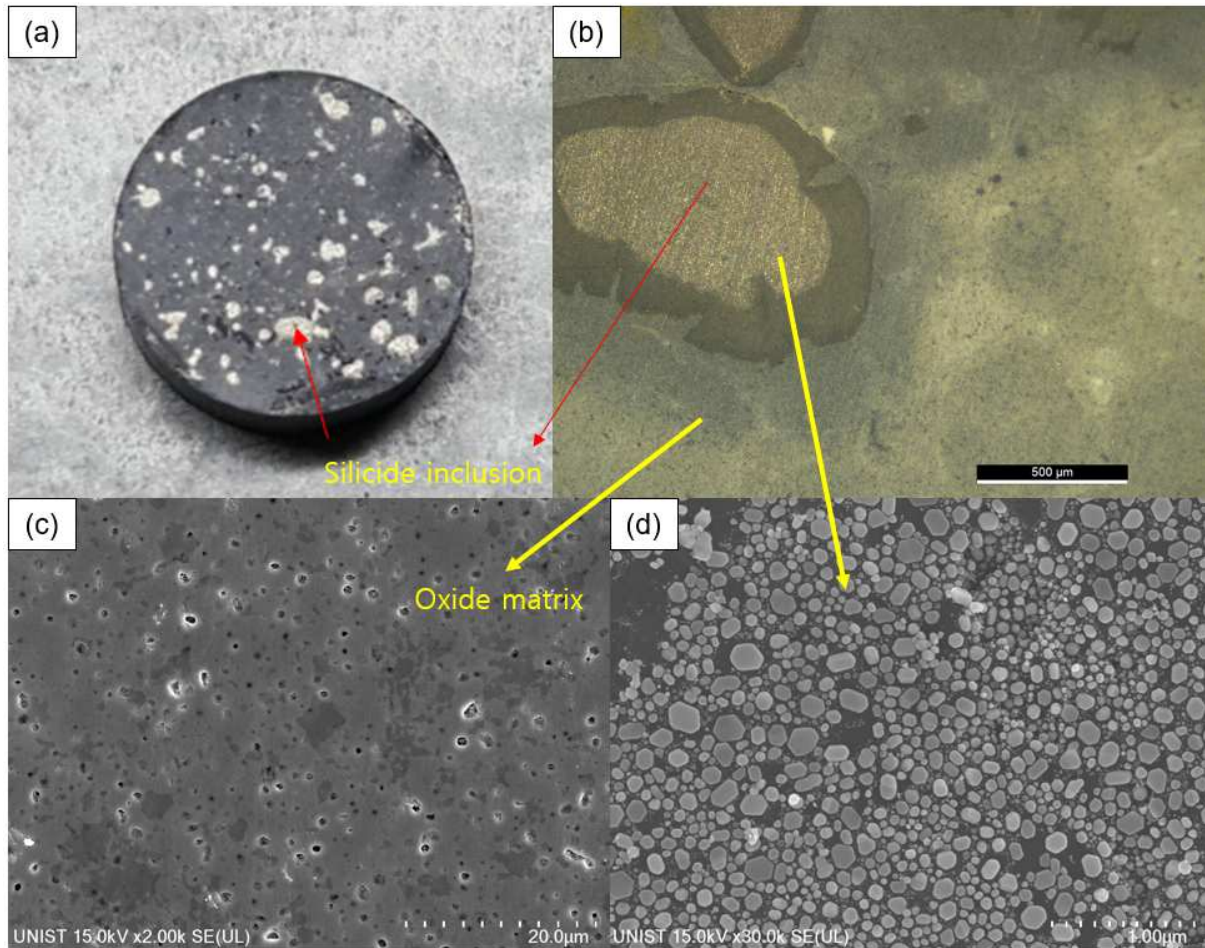


Figure 6: Microstructure of  $\text{CeO}_2$ -30 wt%  $\text{Ce}_3\text{Si}_2$  composites sintered by CS at 1600 °C for 6 hours. (a) cross section of pellet, (b) OM image, (c) SEM image of oxide matrix, and (d) silicide inclusion.

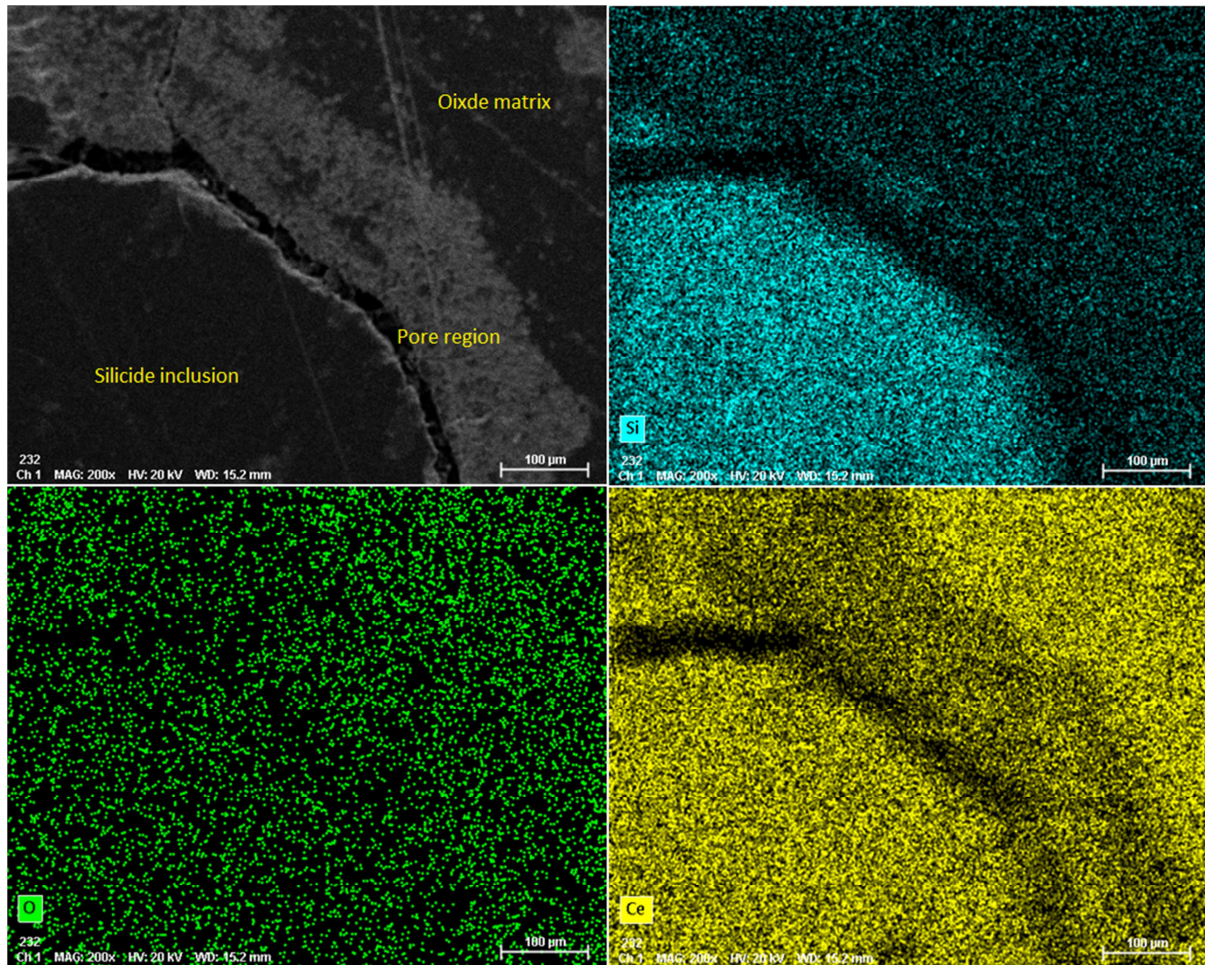


Figure 7: EDS mapping image of  $\text{CeO}_2$ -30 wt%  $\text{Ce}_3\text{Si}_2$  composites sintered by CS at 1600 °C for 6 hours.

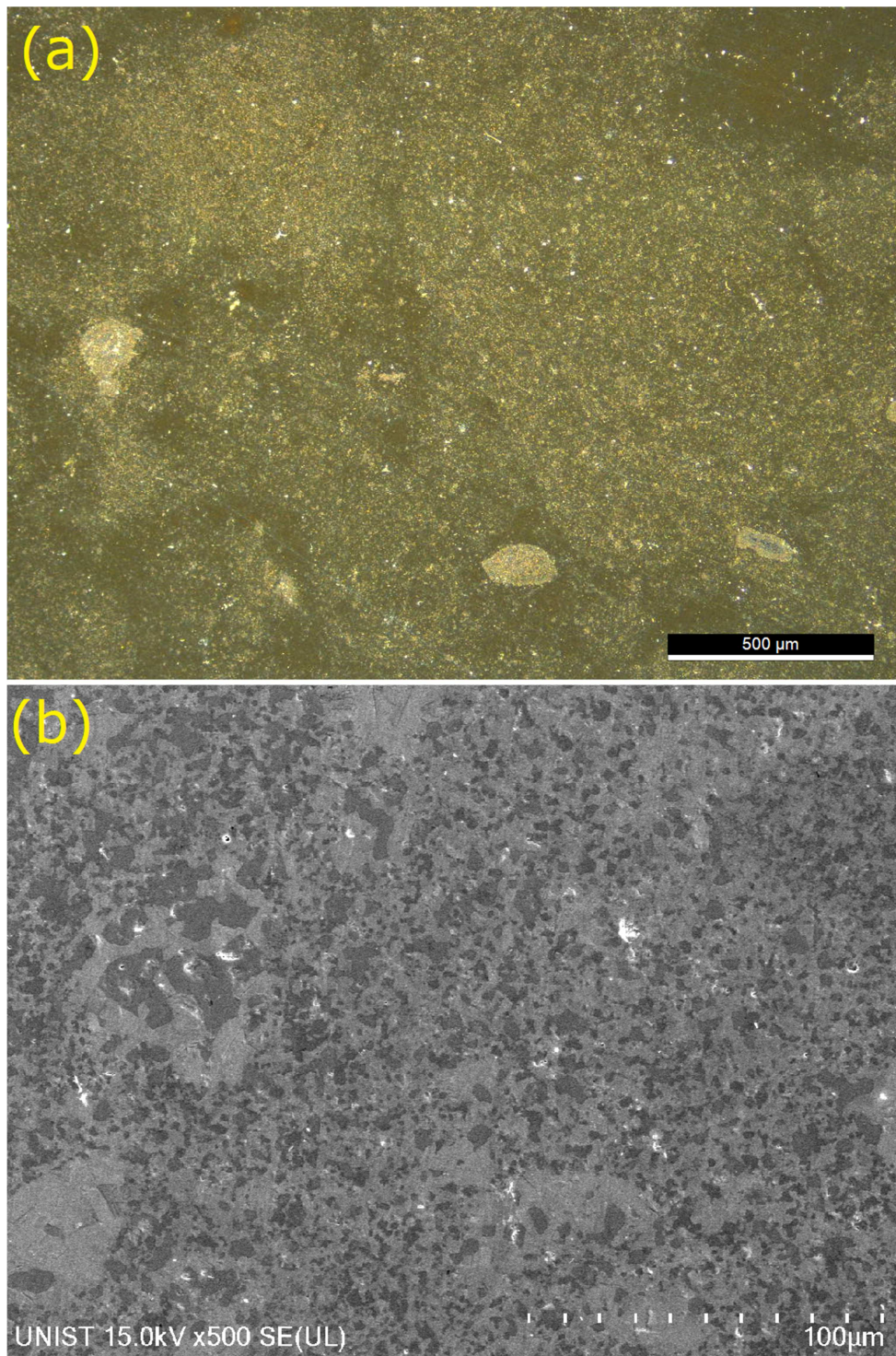


Figure 8: Microstructure of  $\text{CeO}_2$ -30 wt%  $\text{Ce}_3\text{Si}_2$  composite sintered by SPS at 1400 °C for 10 min. (a) OM image, and (b) SEM image.

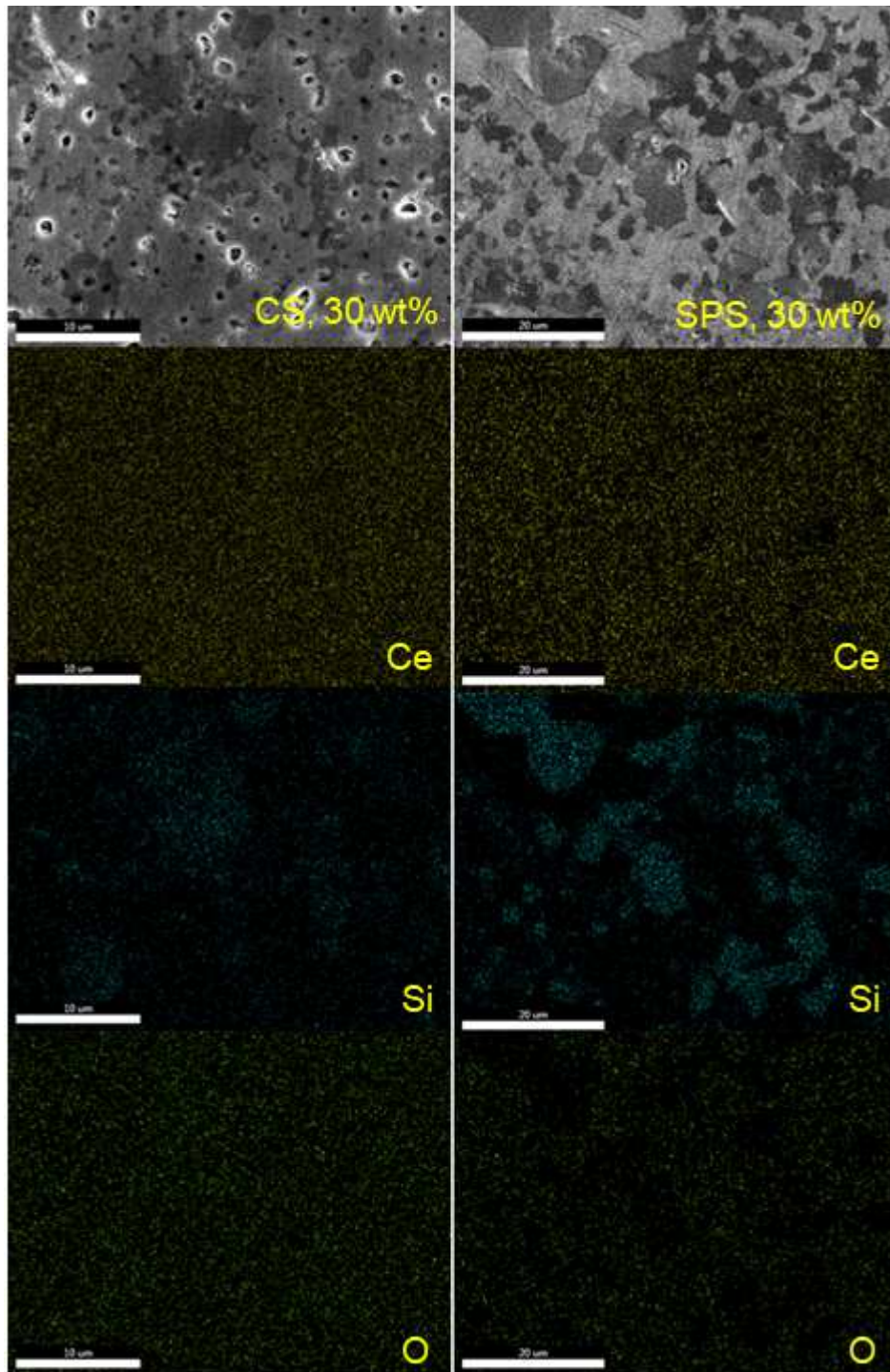


Figure 9: EDS mapping image of  $\text{CeO}_2$ -30 wt%  $\text{Ce}_3\text{Si}_2$  composite sintered by CS at 1600 °C for 6 hours and SPS at 1400 °C for 10 minutes.

### 3.2 Thermal conductivity of $\text{CeO}_2$ - $\text{Ce}_3\text{Si}_2$ composites

Thermal conductivity and specific heat capacity of the composites was only measured from the SPS pellets considering more homogeneous and dense microstructures shown in Figs. 8 and 9. The measured thermal conductivities of  $\text{CeO}_2\text{-}x\text{Ce}_3\text{Si}_2$  ( $x = 0, 10, 30, 50,$  and  $100$  wt%) composites are summarized in Table 1. Thermal conductivities of  $\text{CeO}_2$  ( $4.9$  W/m-K) and  $\text{Ce}_3\text{Si}_2$  ( $5.4$  W/m-K) are similar at room temperature; however, with increasing temperature, increasing thermal conductivity of  $\text{Ce}_3\text{Si}_2$  ( $8.3$  W/m-K) reaches  $\sim 5.7$  times higher value than that of  $\text{CeO}_2$  ( $1.9$  W/m-K) at  $1000$  °C, which well resembles the temperature dependency of  $\text{UO}_2$  and  $\text{U}_3\text{Si}_2$  thermal conductivities [3, 16]. Enhanced thermal conductivity of the composites for high temperature regime ( $> 300$  °C) also can be confirmed from Fig. 10, even despite the higher relative density of  $\text{CeO}_2$  pellet than those of composite pellets. Quantitative comparisons between thermal conductivities of the composites and  $\text{CeO}_2$  are summarized in Table 2.

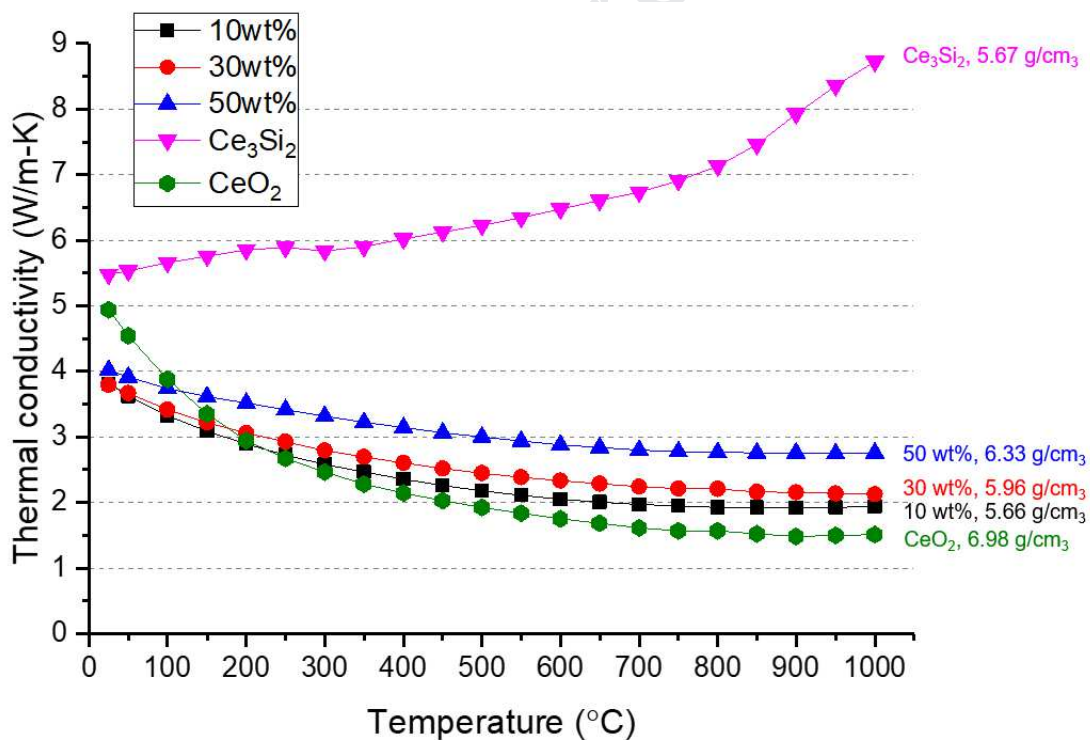


Figure 10: Thermal conductivity of  $\text{CeO}_2\text{-}x\text{Ce}_3\text{Si}_2$  ( $x = 0, 10, 30, 50,$  and  $100$  wt%) sintered by SPS at  $1400$  °C for  $10$  min in vacuum. Part of the  $\text{CeO}_2$  matrix was converted to  $\text{Ce}_2\text{O}_3$  due to the reducible environment.

**Table 1** Thermal conductivity and specific heat capacity of CeO<sub>2</sub>-Ce<sub>3</sub>Si<sub>2</sub> composite pellets sintered by SPS with varying Ce<sub>3</sub>Si<sub>2</sub> composition.

Composition (wt%Ce <sub>3</sub> Si <sub>2</sub> )	0	10	30	50	100	0	10	30	50	100
Temperature (°C)	Thermal conductivity (W/m-K)					Specific heat capacity (J/g-K)				
50	4.54	3.62	3.46	3.92	5.53	0.36	0.42	0.38	0.37	0.36
100	3.88	3.33	3.24	3.74	5.66	0.39	0.42	0.38	0.38	0.36
150	3.35	3.09	3.06	3.62	5.76	0.40	0.43	0.39	0.39	0.36
200	2.94	2.89	2.92	3.52	5.85	0.41	0.44	0.40	0.39	0.37
250	2.67	2.73	2.81	3.41	5.89	0.42	0.44	0.40	0.40	0.37
300	2.47	2.58	2.73	3.32	5.84	0.43	0.45	0.41	0.40	0.37
350	2.28	2.47	2.60	3.23	5.90	0.43	0.45	0.42	0.40	0.38
400	2.15	2.36	2.52	3.14	6.02	0.44	0.46	0.42	0.41	0.38
450	2.02	2.26	2.46	3.07	6.12	0.44	0.47	0.43	0.41	0.38
500	1.92	2.18	2.37	3.00	6.23	0.44	0.47	0.43	0.42	0.39
550	1.84	2.11	2.31	2.94	6.35	0.44	0.48	0.44	0.42	0.39
600	1.75	2.05	2.25	2.88	6.47	0.44	0.48	0.44	0.42	0.39
650	1.68	2.01	2.21	2.84	6.61	0.45	0.49	0.45	0.43	0.40
700	1.61	1.97	2.18	2.80	6.74	0.45	0.49	0.45	0.43	0.40
750	1.56	1.95	2.14	2.78	6.90	0.45	0.50	0.46	0.43	0.40
800	1.57	1.93	2.12	2.77	7.13	0.46	0.50	0.47	0.44	0.40
850	1.52	1.93	2.11	2.76	7.46	0.46	0.51	0.47	0.44	0.40
900	1.48	1.92	2.09	2.76	7.93	0.46	0.52	0.48	0.45	0.40
950	1.49	1.93	2.09	2.75	8.36	0.46	0.52	0.48	0.46	0.40
1000	1.51	1.94	2.09	2.76	8.73	0.47	0.53	0.49	0.46	0.40



**Table 2** Thermal conductivity change of  $\text{CeO}_2\text{-}x\text{Ce}_3\text{Si}_2$  ( $x = 10, 30, \text{ and } 50$  wt%) composite

Temperature (°C)	Silicide composition (wt%)		
	10	30	50
	Thermal conductivity change (%)		
25	-22.84	-23.14	-18.61
100	-14.35	-12.08	-3.69
200	-1.68	4.29	19.51
300	4.80	13.32	34.53
400	9.45	21.38	46.00
500	13.26	27.81	56.09
600	17.67	34.30	65.27
700	22.28	39.64	73.67
800	23.21	40.27	76.81

pellets compare to  $\text{CeO}_2$ , sintered by SPS at 1400 °C.

900	29.47	46.31	85.78
1000	27.83	41.91	81.54

Journal Pre-proof

#### 4. Discussion

From the XRD diffraction pattern shown in Fig. 4,  $\text{Ce}_2\text{O}_3$  peaks, rather than  $\text{CeO}_2$ , were observed in both CS and SPS pellets. This reduction of the oxide was anticipated considering easily reducing environment of  $\text{CeO}_2$  such as high temperature, oxidizing of  $\text{Ce}_x\text{Si}_y$  and the aforementioned sintering atmosphere, vacuum for SPS and argon for CS [17-19]. However, these reductive sintering conditions were unavoidable to not oxidize the silicide since the goal of this study was to quantify the thermal conductivity enhancement effect from  $\text{Ce}_3\text{Si}_2$  addition.

In the standpoint of establishing the fabrication process for  $\text{UO}_2\text{-U}_3\text{Si}_2$  composite, Fig. 5 shows four important points: (1) SPS pellets always exhibited higher relative density compared to CS, regardless of silicide composition and sintering temperature; (2) relatively low sintering temperature ( $\sim 1400\text{ }^\circ\text{C}$ ) was enough for SPS to achieve high relative density ( $> 90\text{ \%TD}$ ); (3) higher sintering temperature ( $> 1600\text{ }^\circ\text{C}$ ) was required for CS to achieve the same level of high density; (4) for both sintering methods, higher relative density was achieved with higher silicide contents, perhaps largely indebted to high melting temperature of  $\text{CeO}_2$  and low temperature densification of  $\text{Ce}_3\text{Si}_2$  [20-24]. The reason for high density of SPS pellets might be not only the high sintering performance of SPS, but also the actual temperature is higher than the measured temperature. The radial temperature gradient from mold surface to center exists and the pyrometer measured only the mold surface temperature. [25, 26]. Even considering the fact above, however, SPS pellets already has fully compacted at  $1200\text{ }^\circ\text{C}$  of measured sintering temperature, which suggests that fact, the actual sintering temperature in SPS is higher than the measured temperature, has no significant effect of pellet density in this experiment.

Large silicon-rich inclusions, interaction area, and crack shown in Fig. 6(b) and Fig. 7 were discovered from all compositions of CS pellets sintered at  $1600\text{ }^\circ\text{C}$ , which consisting of numerous hexagonal submicron precipitates as shown in Fig. 6(d). Smaller precipitate size than that of the starting  $\text{Ce}_3\text{Si}_2$  powder may imply that their formation was by the congruent melting of  $\text{Ce}_3\text{Si}_2$  at  $1390\text{ }^\circ\text{C}$  and its sequential agglomeration [7]. This type of complex microstructure such as inhomogeneous silicide agglomeration and 2<sup>nd</sup> phase formation in

high temperature sintered CS pellets could be potential performance and safety issues for the  $\text{UO}_2\text{-U}_3\text{Si}_2$  fuel, especially during daily load following operation incurring more frequent thermal cycling of the fuel. Differential thermal expansion coefficients of the silicide agglomeration, secondary phases, and the oxide bulk could facilitate additional fuel cracking, other than typical radial cracking in conventional  $\text{UO}_2$  fuel [27, 28]. This additional mode of cracking could decrease effective fuel thermal conductivity and increase stress concentration on zircaloy cladding via pellet-cladding mechanical interaction. The SPS pellets, on the contrary, relatively showed more homogeneous distribution of  $\text{CeO}_2$  and  $\text{Ce}_3\text{Si}_2$  as shown in Fig. 8, likely resulted from 36 times shorter holding time (10 min) at lower sintering temperature (1400 °C), compared to 6 h and 1600 °C for CS pellets.

Density-wise, despite the remarkable increase of CS pellet densities by the liquid phase sintering with increasing sintering temperature, obtained relative densities of 10 wt%  $\text{Ce}_3\text{Si}_2$  composites are still below 90 %TD for all sintering temperatures. For 30 and 50 wt% composites, only the highest temperature (1600 °C) CS gives over 90 %TD. In contrast, 1200 °C SPS already achieved over 90 %TD, except 10 wt% pellets, which indicates the congruent melting issue at 1390 °C in CS can be avoided using SPS. Thus, thermal conductivity database of  $\text{UO}_2\text{-U}_3\text{Si}_2$  composites can be more reliably constructed utilizing low temperature SPS, especially for silicide-rich ( $\geq 30$  wt%) compositions.

Another superior characteristic of SPS, suppressed interdiffusion of oxygen and silicon between the two-phase boundary, can be designated from the EDS results shown in Fig 9. Relatively enhanced interdiffusion of non-metallic elements in CS composites reaffirmed the decision to not measure the thermal conductivity of CS pellets with low relative density ( $< 80$  %TD) for lower sintering temperature ( $\leq 1400$  °C) and the congruent melting for the high sintering temperature (1600 °C). However, conventional sintering will still be considered for the further study on uranium-bearing composite, since the congruent melting of  $\text{U}_3\text{Si}_2$  occurs at 1660 °C and therefore less severe agglomeration and secondary phase formation are expected for  $\text{UO}_2\text{-U}_3\text{Si}_2$  binary system.

Figure 10 indicates that the thermal conductivity of the composites is actually lower than pure  $\text{CeO}_2$  for low temperature region ( $< \sim 250$  °C). The cerium dioxide can be easily converted to  $\text{CeO}_{2-x}$  or  $\text{Ce}_2\text{O}_3$  at reducible environment such as the presence of  $\text{Ce}_x\text{Si}_y$  nearby,

which is verified by the  $\text{Ce}_2\text{O}_3$  peak shown in Fig. 4. The thermal conductivity of  $\text{CeO}_2$  is dominantly determined by the phonon scattering at the low temperature range. The oxygen vacancy from hypo-stoichiometry phase can interfere with phonon transfer, which resulted in lower thermal conductivity. The thermal conductivity tendency as  $\text{Ce}_3\text{Si}_2$  fraction is flipped for all composites for high temperature region by the significantly higher thermal conductivity of  $\text{Ce}_3\text{Si}_2$  itself, which collectively are a suitable characteristic as a nuclear fuel. Most notably, 50 wt%  $\text{Ce}_3\text{Si}_2$  composite exhibited 55% higher value at 500 °C and 81% higher value at 1000 °C.

This thermal conductivity enhancement of the surrogate composites would be much more significant for  $\text{UO}_2\text{-U}_3\text{Si}_2$  composites mainly due to two following reasons. First, the reduction of  $\text{CeO}_2$  during the fabrication prohibited the thermal conductivity enhancement of the composites; however,  $\text{UO}_2$  stoichiometry decrease under high temperature reductive environment is very limited in comparison to that of  $\text{CeO}_2$  [17, 29]. Second,  $\text{U}_3\text{Si}_2$  has 11% higher density ( $12.2 \text{ g/cm}^3$ ) than  $\text{UO}_2$  ( $10.96 \text{ g/cm}^3$ ), unlike 17% lower density of  $\text{Ce}_3\text{Si}_2$  ( $5.97 \text{ g/cm}^3$ ) than that of  $\text{CeO}_2$  ( $7.22 \text{ g/cm}^3$ ). This indicates that the thermal conductivity enhancement of the  $\text{CeO}_2\text{-Ce}_3\text{Si}_2$  composites was determined by higher thermal conductivity of  $\text{Ce}_3\text{Si}_2$  and the reduction of  $\text{CeO}_2$ . Additional thermal conductivity enhancement can thus be expected from  $\text{UO}_2\text{-U}_3\text{Si}_2$  composites due to stoichiometric  $\text{UO}_2$  and further increased density by silicide compositing.

## 5. Conclusion

Various compositions of non-radioactive surrogate composites,  $\text{CeO}_2\text{-}x\text{Ce}_3\text{Si}_2$  ( $x = 0, 10, 30, 50, \text{ and } 100 \text{ wt\%}$ ) were fabricated using conventional sintering and spark plasma sintering in order to effectively construct the thermal conductivity database of  $\text{UO}_2\text{-U}_3\text{Si}_2$  nuclear fuel with minimum uranium-bearing waste generation. Thermal conductivity of the composites was measured from spark plasma sintered pellets due to their homogeneous microstructure and high relative density ( $> 90\% \text{ TD}$ ). Silicide agglomerations and enhanced interdiffusion of oxygen and silicon observed from conventionally-sintered pellets, which could be potential safety issue, were additional reasons to exclude the CS pellets from the in addition to their low relative densities. Based upon measured thermal conductivity of the surrogate, the  $\text{UO}_2\text{-}$

$U_3Si_2$  composites may be suitable candidates, since  $CeO_2$ -50wt% $Ce_3Si_2$  exhibited up to 81% higher thermal conductivity than pure  $CeO_2$  and even further thermal conductivity enhancement can be expected from  $UO_2$ - $U_3Si_2$  composite due to stoichiometric  $UO_2$  and higher  $U_3Si_2$  density than  $UO_2$ .

### **Acknowledgement**

This research was supported by Basic Science Research Program through the National Research Foundation of Korea (NRF) funded by the Ministry of Science, ICT & Future Planning (No. NRF-2016R1A5A1013919).

## References

- [1] A.A.E. Abdelhameed, X.H. Nguyen, J. Lee, Y. Kim, Feasibility of Passive Autonomous Frequency Control Operation in a Soluble-Boron-Free Small PWR, *Ann. Nucl. Energy*. 116 (2018) 319–333.
- [2] E.S. Solntceva, M.L. Taubin, V.I. Vybyvanets, I.E. Galyov, V.G. Baranov, O. V. Homyakov, A. V. Tennishev, Thermal Conductivity of Perspective Fuel Based on Uranium Nitride, *Ann. Nucl. Energy*. 87 (2016) 799–802.
- [3] J.T. White, A.T. Nelson, J.T. Dunwoody, D.D. Byler, D.J. Safarik, K.J. McClellan, Thermophysical Properties of  $U_3Si_2$  to 1773 K, *J. Nucl. Mater.* 464 (2015) 275–280.
- [4] R. De Coninck, W. Van Lierde, A. Gijs, Uranium Carbide: Thermal Diffusivity, Thermal Conductivity and Spectral Emissivity at High Temperatures, *J. Nucl. Mater.* 57 (1975) 69–76.
- [5] B.T.M. Willis. Structures of  $UO_2$ ,  $UO_{2+x}$  and  $U_4O_9$  by Neutron Diffraction. *Journal de Physique*, 1964, 25 (5), pp.431-439.
- [6] A. Bumajdad, J. Eastoe, A. Mathew, Cerium Oxide Nanoparticles Prepared in Self-assembled Systems, *Adv. Colloid Interface Sci.* 147–148 (2009) 56–66.
- [7] B.A. Munitz, A.B. Gokhale, G.J. Abbaschian, The Ce-Si ( Cerium-Silicon ) System, 10 (1989) 73–78.
- [8] J. Rosales, Characterization of  $U_3Si_2$  Surrogates to Predict  $U_3Si_2$  Additive Manufactured Microstructures, 2018.
- [9] R.K. Viswanadham, S.K. Mannan, S. Kumar, M.M. Laboratories, Mechanical Alloying Behavior in Group V Transition Metal/Silicon Systems, *Scr. Metall.* 22 (1988) 1011–1014.
- [10] S. Yagoubi, S. Heathman, A. Svane, G. Vaitheeswaran, P. Heines, J.C. Griveau, T. Le Bihan, M. Idiri, F. Wastin, R. Caciuffo, High Pressure Studies on Uranium and Thorium Silicide Compounds: Experiment and Theory, *J. Alloys Compd.* 546 (2013)..
- [11] J. Roleček, Š. Foral, K. Katovský, D. Salamon, A Feasibility Study of Using  $CeO_2$  as a Surrogate Material During the Investigation of  $UO_2$  Thermal Conductivity Enhancement, *Adv. Appl. Ceram.* 116 (2017) 123–131.
- [12] G.A. Alanko, B. Jaques, A. Bateman, D.P. Butt, Mechanochemical Synthesis and Spark Plasma Sintering of the Cerium Silicides, *J. Alloys Compd.* 616 (2014) 306–311.
- [13] James Blanchard, D. Butt, M. Meyer, P. Xu, Development of Advanced High Uranium Density Fuels for Light Water Reactors, 2016.
- [14] G.A. Alanko, D.P. Butt, Mechanochemical Synthesis of Uranium Sesquisilicide, *J. Nucl. Mater.* 451 (2014) 243–248.
- [15] FIZ Karlsruhe. Germany, ICSD - Inorganic Crystal Structure Database

- [16] Y. Kim, J. Park, J. Cleveland, Thermophysical Properties Database of Materials for Light Water Reactors and Heavy Water Reactors, 2006.
- [17] D.R. Mullins, The Surface Chemistry of Cerium Oxide, 2014.
- [18] R.A. Prasad, Spark Plasma Sintering of Cerium Dioxide and its Composites, 2017.
- [19] D. Galusek, K. Ghillányová, Ceramic Oxides, Ceram. Sci. Technol. Vol. 2 Mater. Prop., 2010.
- [20] T. Zhang, P. Hing, H. Huang, J. Kilner, Sintering Study on Commercial CeO<sub>2</sub> Powder with Small Amount of MnO<sub>2</sub> Doping, Mater. Lett. 57 (2002) 507–512..
- [21] Y.C. Zhou, Hydrothermal Synthesis and Sintering of Ultrafine CeO<sub>2</sub> Powders, J. Mater. Res. 8 (1993) 1680–1686.
- [22] P.A. Lessing, Oxidation Protection of Uranium Nitride Fuel Using Liquid Phase Sintering," 2012
- [23] K.D. Johnson, A.M. Raftery, D.A. Lopes, J. Wallenius, Fabrication and microstructural analysis of UN-U<sub>3</sub>Si<sub>2</sub> composites for accident tolerant fuel applications, J. Nucl. Mater. 477 (2016) 18–23.
- [24] J.T. White, A.W. Travis, J.T. Dunwoody, A.T. Nelson, Fabrication and thermophysical property characterization of UN/U<sub>3</sub>Si<sub>2</sub> composite fuel forms, J. Nucl. Mater. 495 (2017) 463–474.
- [25] G. Lee, E.A. Olevsky, C. Manière, A. Maximenko, O. Izhevskiy, C. Back, J. Mckittrick, Effect of electric current on densification behavior of conductive ceramic powders consolidated by spark plasma sintering Acta Materialia Effect of electric current on densification behavior of conductive ceramic powders consolidated by spark plasma sintering, Acta Mater. 144 (2017) 524–533.
- [26] Y. Achenani, M. Saâdaoui, A. Cheddadi, G. Bonnefont, G. Fantozzi, Finite element modeling of spark plasma sintering : Application to the reduction of temperature inhomogeneities , case of alumina, JMADE. 116 (2016) 504–514.
- [27] E.S. Folias, M. Hohn, T. Nicholas, Predicting Crack Initiation in Composite Material Systems due to a Thermal Expansion Mismatch, Int. J. Fract. 93 (1998) 335–349.
- [28] F. Delale, H. Boduroglu, Effect of Thermal Expansion Anisotropy on Microcracking in Ceramic Composites, Eng. Fract. Mech. 39 (1991) 45–60.
- [29] J Williams, Sintering of Uranium Oxides of Composition UO<sub>2</sub> to U<sub>3</sub>O<sub>8</sub> in Various Atmospheres, J. Nucl. Mater. 1 (1959) 28–38.



**Declaration of interests**

The authors declare that they have no known competing financial interests or personal relationships that could have appeared to influence the work reported in this paper.

The authors declare the following financial interests/personal relationships which may be considered as potential competing interests: